Contrib Mineral Petrol (2006) 152:485–503
DOI 10.1007/s00410-006-0116-1

ORIGINAL PAPER

Composition and origin of fluids associated with lode gold deposits in a Mesoarchean greenstone belt (Warrawoona Syncline, Pilbara Craton, Western Australia) using synchrotron radiation X-ray fluorescence

Nicolas Thébaud · Pascal Philippot · Patrice Rey · Jean Cauzid

Received: 25 November 2005 / Accepted: 6 June 2006 / Published online: 18 July 2006

Abstract Microthermometry and Raman spectroscopy techniques are routinely use to constrain ore-fluids $\delta^{18}O$ and molar proportions of anhydrous gas species (CO_2, CH_4, N_2). However, these methods remain imprecise concerning the ore-fluids composition and source. Synchrotron radiation X-ray fluorescence allows access to major and trace element concentrations (Cl, Br and K, Ca, Fe, Cu, Zn, As, Rb, Sr) of single fluid inclusion. In this paper, we present the results of the combination of these routine and newly developed techniques in order to document the fluids composition and source associated with a Mesoarchaean lode gold deposit (Warrawoona Syncline, Western Australia). Fluid inclusion analyses show that quartz veins preserved records of three fluid inclusion populations. Early fluids inclusions, related to quartz veins precipitation, are characterized by a moderate to high Br/Cl ratio relative to modern seawater, $CO_2 \pm CH_4 \pm N_2$, low to moderate salinities and significant base metal (Fe, Cu, Zn) and metalloid (As) concentrations. Late fluid inclusions trapped in secondary aqueous fluid inclusions are divided into two populations with distinct compositions. The first population consists of moderately saline aqueous brines, with a Br/Cl ratio close to modern seawater and a low concentration of base metals and metalloids. The second population is a fluid of low to moderate salinity, with a low Br/Cl ratio relative to modern seawater and significant enrichment in Fe, Zn, Sr and Rb. These three fluid inclusion populations point to three contrasting sources: (1) a carbonic fluid of mixed metamorphic and magmatic origin associated with the gold-bearing quartz precipitation; (2) a secondary aqueous fluid with seawater affinity; and (3) a surface-derived secondary aqueous fluid modified through interaction with felsic lithologies, before being flushed into the syncline. Primary carbonic fluids present similar characteristics than those ascribed to Mesoarchaean lode gold deposits. This suggests similar mineralization processes for mid- and Mesoarchaean lode gold deposits despite contrasting fluid–rock interaction histories. However, in regard to the protracted history documented in the Warrawoona Syncline, we question the robustness of the epigenetic crustal continuum model, as ore-fluid characteristics equally support an epigenetic or a polyphased mineralization process.

Keywords Fluid inclusion composition · Pilbara · Synchrotron · Gold deposit · Mesoarchaean

Communicated by J. Hoefs

N. Thébaud (✉) · P. Philippot
Institut de Physique du Globe de Paris, Laboratoire Géobiosphère Actuelle et Primitive, CNRS UMR 7154, case 89, Tour 14-15 4 place Jussieu, 75252 Paris Cedex 5, France
e-mail: nicolas.thebaud@gmail.com

P. Rey · N. Thébaud
School of Geosciences, H11 Geology Demountables, University of Sydney, Sydney, NSW 2006, Australia

J. Cauzid
European Synchrotron Radiation Facility, ID 22, 6 rue Jules Horowitz, BP220, 38043 Grenoble Cedex, France

Introduction

With a total production of 2.2 Moz Au until 2000, the early to Mesoarchean terrane of the Pilbara Craton in

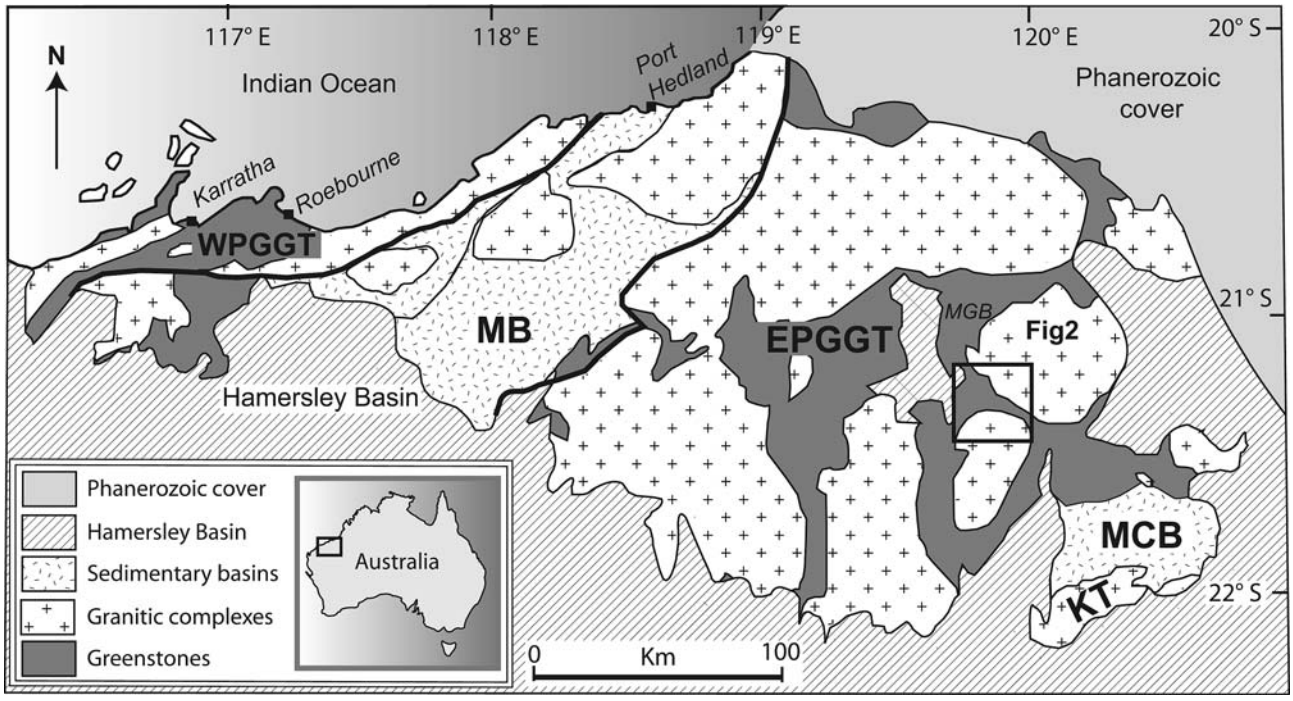

Fig. 1 Simplified geological map of the North Pilbara terrane modified after Van Kranendonk et al. (2002). *EPGGT* East Pilbara Granite–Greenstone Terrane, *CPTZ* Central Pilbara Tectonic Zone, *WPGGT* West Pilbara Granite–Greenstone Terrane, *MB* Mallina Basin, *MCB* Mosquito Creek Basin, *KT* Kuranna Terrane, *MGB* Marble Bar Greenstone Belt

Western Australia (Fig. 1) has historically shown lower Au production in comparison to the Neoarchaean Eastern Goldfields Province of the Yilgarn Craton in Western Australia (130 Moz Au until 2000; Goldfarb et al. 2001; Huston et al. 2001). As a result, most of the lode gold mineralization studies have been conducted within Neoarchaean, Yilgarn Craton leaving Mesoarchean terrane relatively unexplored. Archaean lode gold mineralizations represent a coherent class of gold deposit called 'orogenic gold deposit' that developed over a crustal depth range from granulite to subgreenschist facies environments (crustal continuum model; Groves 1993). According to this model, gold mineralization resulted from a syn-tectonic epigenetic emplacement process associated with fluids channelled along crustal-scale shear zones (Goldfarb et al. 2001; Groves 1993; Kerrich and Wyman 1990). Fluid inclusions and stable isotopes studies supporting this interpretation remain uncertain concerning the source and composition of the ore-related fluid, suggesting either a surface-derived, or a metamorphic, or a magmatic fluid (Groves and Phillips 1987; McCuaig and Kerrich 1998). Multi-techniques including μ-SR-XRF are essential to further constrain the source and composition of ore fluids. This paper documents the composition and the origin of the fluids associated with the lode-gold within the Warrawoona Syncline in the Eastern Pilbara (EPGGT, Fig. 1). Our multi-techniques analytical approach shows that quartz veins preserve the fingerprints of three main stages of fluid infiltration involving a primary aqueous-carbonic fluid of deep origin (magmatic and/or metamorphic) and two aqueous fluids of surficial origin. Based on our data set, we show that the fluid chemistry and quartz isotopic composition associated with gold deposit from the Mesoarchean Warrawoona Syncline are similar to that of far more richly endowed Neoarchaean orogenic gold deposits.

General setting

Geological and structural setting

The Pilbara Craton (Western Australia) is a well-exposed 3.6–2.8 Ga granite–greenstone terrane overlain by volcanic and sedimentary rocks of the Hamersley Basin (2.77–2.40 Ga, Fig. 1). The East Pilbara Granite–Greenstone Terrane (EPGGT, Figure 1) is characterized by circular to elliptic granitic domes, 40–120 km in diameter, encircled by variably deformed greenstone belts. Granitic domes include 3.46 to 3.43-Ga-old TTG gneisses and younger syn-kinematic and post-kinematic suites of high-K granitic rocks emplaced

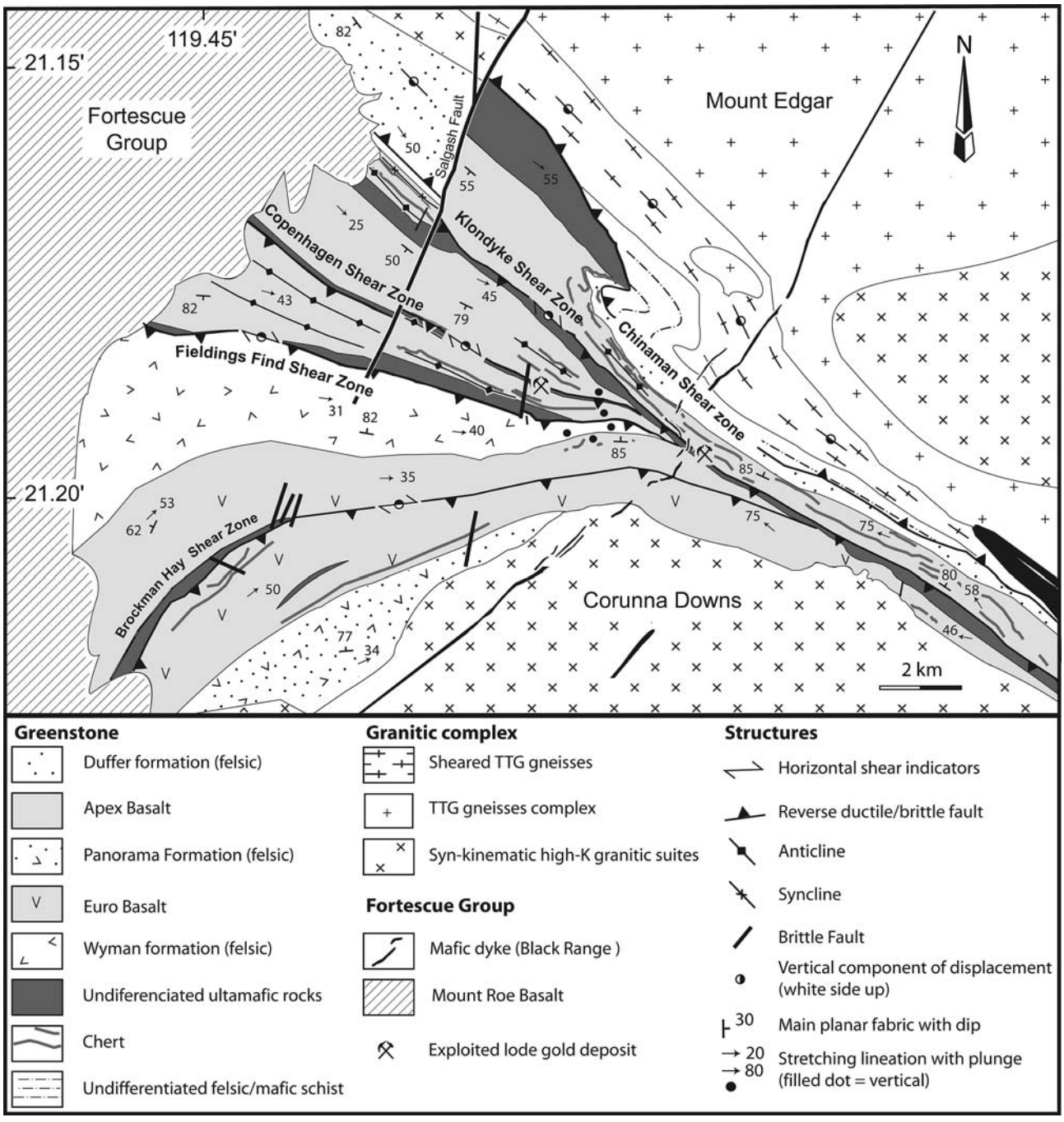

Fig. 2 The study area in the Warrawoona Syncline. Geological map of the Warrawoona Syncline

between 3.32 and 3.30 Ga (Fig. 2) and derived through partial melting of the early TTG (Hickman and Van Kranendonk 2004; Smithies et al. 2003; Van Kranendonk et al. 2002).

Gold-bearing quartz veins from the Warrawoona Syncline are the focus of this study. The Warrawoona Syncline is located between the Mount Edgar and Corunna Downs Granitic Complexes (Fig. 2) and consists of ultramafic, mafic and felsic volcanic rocks and minor sedimentary and chert units that are ascribed to the ca. 3.51–3.43 Ga Warrawoona Group and 3.35–3.31 Ga Kelly Group (Hickman 1983, 2001; Van Kranendonk et al. 2004). The volcanic rocks preserve primary igneous features such as pillows, vesicules and spinifex textures. Facing directions on both limbs point away from the granitic complexes towards the core of the syncline (Hickman 1983, 2001). This syncline is asymmetric, with limbs involving rocks of

contrasting ages, metamorphic facies and strain intensities. On the northern limb, intensely deformed amphibolite facies mafic and felsic schists of the lower part of the Warrawoona Group are in contact with the southern margin of the Mount Edgar Granitic Complex across a kilometre-scale shear zone. The southern limb consists of the upper part of the Warrawoona Group and the overlying Kelly Group. The southern limb is intruded by ca. 3.30 Ga granitic rocks of the Corunna Downs Granitic Complex.

At a regional scale, the Warrawoona Syncline shows a main, steeply dipping, foliation (S_m) parallel to the granitic/greenstone boundaries. A pronounced mineral and stretching lineation (L_m) rotates and converges toward a small area where the lineation is vertical (Collins et al. 1998; Teyssier et al. 1990; Zegers et al. 2002; Fig. 2). The finite strain ellipsoid changes from S tectonites near the contact with the granitic complexes to L tectonites where L_m is vertical (Collins et al. 1998; Teyssier et al. 1990; Zegers et al. 2002). Open to isoclinal folds occur at all scales. Folds axial planes are parallel to S_m and fold axes are parallel to L_m (Fig. 2). Locally, later folds refold these regional fabrics.

The S and SW rim of the Mount Edgar is affected by a kilometric-scale shear zone (Fig. 2) with down-dip stretching lineation. Kinematic analysis reveals that the shear zone accommodated the exhumation of the granitic dome (Collins 1989; Collins et al. 1998; Teyssier et al. 1990). Within the greenstones, hectometre to kilometre-scale shear zones involve oblique horizontal dextral and sinistral sense of shear generating pop-up structures (Kloppenburg et al. 2001). As the stretching lineation rotates to become vertical and the finite strain ellipsoid evolves to constriction, the horizontal shear component disappears. Radiometric data (U–Pb zircon on syn- and post granites and Ar–Ar on metamorphic fabrics) constrain the age of the formation of the syncline between 3.32 and 3.30 Ga (Collins et al. 1998; Kloppenburg et al. 2001).

Fluid–rock interactions and lode gold mineralization

The Warrawoona Syncline is one of the largest mafic-ultramafic-hosted goldfields in the EPPGT. This district has produced 745 kg of Au from 25 kt of ore, with an average grade of 29.6 g/t, and an additional 22 kg of alluvial Au (Hickman 1983; Huston et al. 2001). More recently, a geological resource of 9.95 Mt at 1.0 g/t has been identified for the Klondyke deposit (Huston et al. 2001). The ore deposits are mainly composed of lodes hosted within kilometric shear zones (Huston et al. 2001). The age of the mineralization is loosely constrained by three Pb model ages from galenas: 3.38, 3.37 and 3.05 Ga (Huston et al. 2001). In a recent study, oxygen isotopic and geochemical analyses on whole rock and quartz veins were combined with structural observations to constrain the fluid circulation and lode gold mineralization history (Thébaud et al. 2006). This study suggests that the Warrawoona Syncline was the locus of a protracted and polyphased fluid circulation history involving at least two stages of paleo-fluid infiltration of contrasted temperatures and sources. Alteration halo around the main shear zone (Fielding's Find Shear Zone) is characterized by an intense silicification, HREE depletion and ^{18}O enrichment. These features are interpreted as the result of an alteration process driven by low-temperature hydrothermal convection probably involving seawater. This first stage was followed by a veining episode related to the syn-tectonic infiltration of deep sourced fluids characterized by quartz veins with quartz $\delta^{18}O$ values centred around a mean value of 13.2‰, significantly lower than their silicified host rocks. These quartz veins represent the event responsible for the bulk of economic lode-gold formation; however, no definitive constraints exist on the ore-fluid source.

Quartz veins

Quartz veins are ubiquitous in the Warrawoona Syncline. Based on cross-cutting relationships, four main quartz vein populations have been identified (Fig. 3).

Type 1 veins (V_1) can be found throughout the Warrawoona Syncline, but are mainly present along shear zones. Up to a few meters long, they are composed of quartz with minor calcite and ankerite frequently replaced by brown Fe-oxides and sulphides. Locally, they host native gold. These veins are parallel to S_m but can be locally boudinaged or folded. These structural features suggest that V_1 were emplaced prior to or during the deformation. Nevertheless, the absence of quartz veins in the less deformed Marble Bar Greenstone Belt (Fig. 1) supports a syn-deformation origin.

In contrast to V_1, type 2 veins (V_2) are oriented at high angle to L_m and therefore perpendicular to S_m. V_2 veins are < 1 m thick extensional fractures occasionally forming *'en échelon'* vein sets and are composed of quartz with minor sulphides. V_2 veins are progressively reoriented following the attitude of the stretching lineation (L_m) (Fig. 4b–d). Locally, quartz fibres are sub-parallel to the stretching lineation suggesting that V_2 formed during the development of L_m and thus, as V_1, can be considered as syn-deformation quartz veins formed in the brittle–ductile domain.

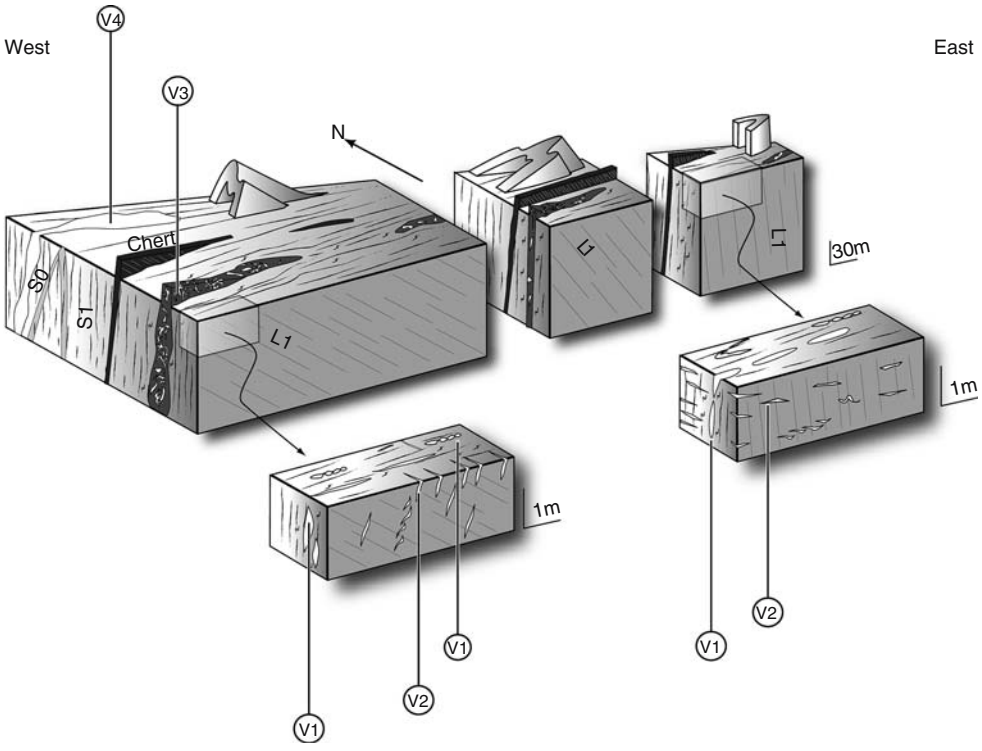

Fig. 3 Sketches of the different structures and associated vein types (V_1–V_4) occurring from west to east in the Warrawoona Syncline. S_0 and S_m refer to local observations of bedding (S_0) and foliation (S_m) relationships (see text)

Type 3 veins (V_3) occur as irregular-shaped breccias forming the core of the shear zones in particular within the Fielding's Find Shear Zone running parallel to the syncline axial surface (Fig. 4e, 4f). V_3 veins consist of pervasive and randomly oriented vein sets within a highly silicified and fuchsite-enriched wall rock. The breccias vary in size but can be followed almost continuously for kilometres along strike, as in the Fielding's Find Shear Zone. The localization of V_3 in the core of the shear zones is best interpreted in terms of a late emplacement possibly associated with hydraulic fracturing during brittle faulting.

Type 4 veins (V_4) form massive quartz pods tens of meters in length (Fig. 4g). Mainly composed of quartz with minor sulphides, they show little to no deformation and occur commonly in mafic material parallel to S1. V_4 is considered to be the result of a late deformation feature postdating the formation of the main shear zones. As fluid inclusions in V_4 were too small to be analysed, they are not integrated in this study.

Analytic approach and methodologies

Our analytical approach relies on the combination of routine geochemical techniques and more recently developed in situ analyses. The combination of microthermometry and Raman spectroscopy provides robust constraints on the inclusion fluid chemistry, including molar proportions of anhydrous gas species (CO_2, CH_4, N_2) and the salinity, as well as constraints on pressure and temperature associated with the (minimal) trapping temperature. μ-SR-XRF techniques were used to constrain the nature and content of solutes (Cl, Br and K, Ca, Fe, Cu, Zn, As, Rb, Sr). Finally, oxygen isotopic analyses were used in conjunction with fluid inclusion analyses to discriminate the various fluid sources.

Microthermometry and Raman spectroscopy

Typology and petrography of fluid inclusions were documented from representative samples of the various quartz vein populations. Microthermometric analyses were performed on fluid inclusions observed in quartz in 16 doubly polished thin sections. Microthermometry was carried out on a Fluid Inc. Modified USGS heating–freezing stage attached to a Leitz Wetzlar Laborlux S binocular microscope. Fluid inclusion types were distinguished using the nomenclature of Boiron et al. (1992). Microthermometric results are presented using the following abbreviations: Tm_{CO2} = melting temperature of solid CO_2; Th_{CO2} = homogenization temperature of CO_2 vapour to the liquid phase; Tmf = final melting temperature of ice or hydrate; Tm_{clath} = melting temperature of

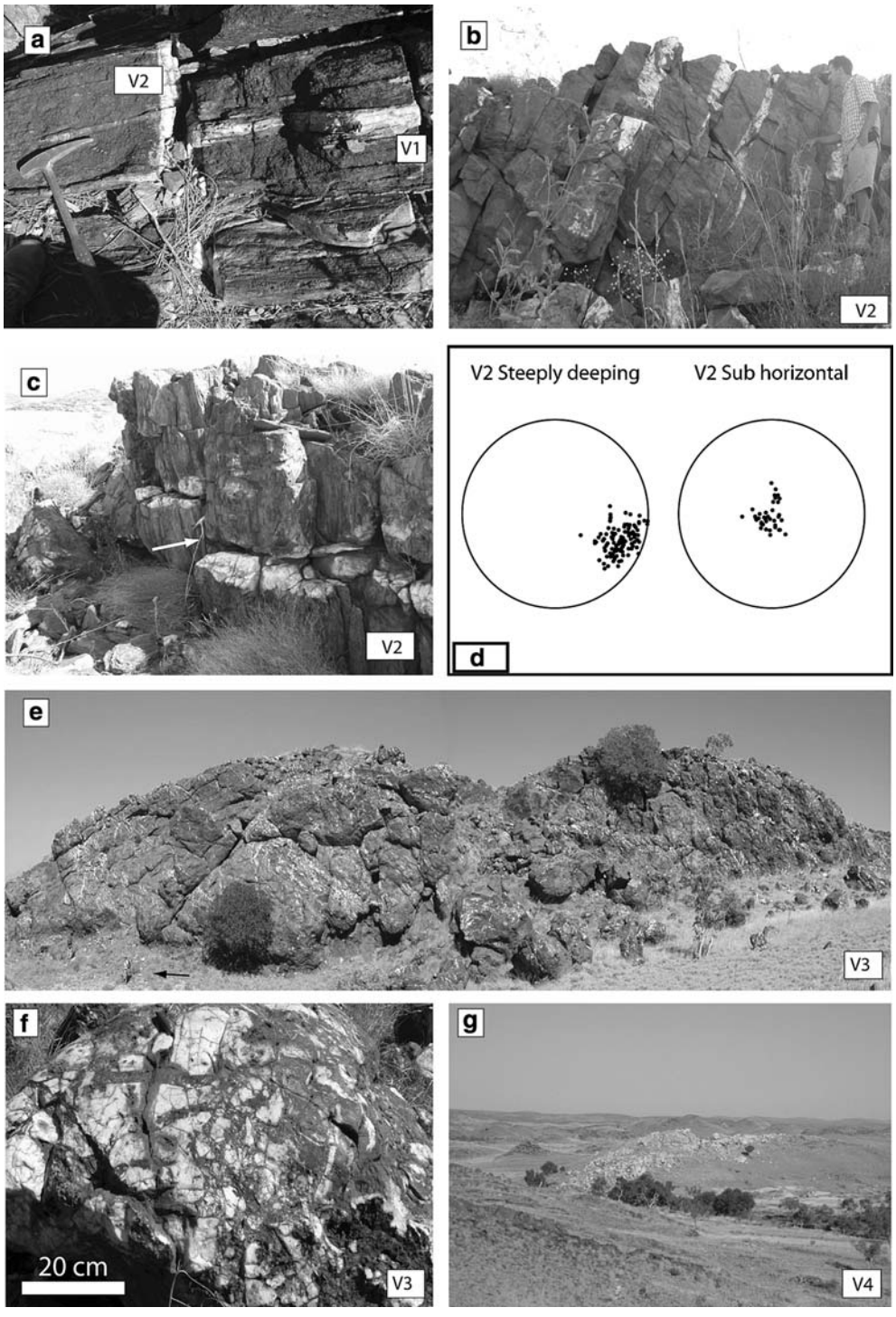

Fig. 4 Outcrop scale photographs of hydrothermal veins encountered in the Warrawoona Syncline. **a** Deformed V_1 quartz vein cross-cut by V_2. **b** View north of steeply west-dipping V_2 extensional quartz veins, plunging ~ 30° toward the ESE at high angle to L_m (toward the person). **c** Sub-horizontal V_2 in the core of the syncline, at high angle to vertical L_m. **d** Stereographic projections of V_2 orientation (poles to planes) from west (*top*) to east (*right*) in the Warrawoona Syncline highlighting the progressive change in orientation from steeply dipping to sub-horizontal toward the core of the Warrawoona Syncline (see text). **e** V_3 breccia vein along Fielding's Find Shear Zone at the outcrop scale; *black arrow* points to a person for scale. **f** Detail of a V_3 breccia vein. **g** V_4 ''massive'' type quartz veins

clathrate; Th = temperature of final homogenization; Td = temperature of decrepitation. The rate of heating was kept under 0.2°C/s during freezing and under 1°C/s during heating. Salinity, expressed as equivalent wt% NaCl, was calculated from microthermometric data using the equation of Bodnar (1993). In vapour-bearing fluid inclusions, the presence of CO_2 amongst other anhydrous phases (CH_4, H_2S) was detected on the basis of the melting temperature of the solid anhydrous phase during freezing and melting cycles. Salinity was calculated using the clathrate melting curves of Collins (1979). The volumetric fraction of the aqueous liquid in carbonic fluid inclusions was estimated using the volumetric chart of Roedder (1972).

Molar fractions of CO_2, CH_4, H_2S and N_2 were determined in individual inclusions by micro-Raman analyses performed with the Labram Raman spectrometer at CREGU at Nancy, France. Bulk compositions and molar volumes were computed from *P–V–T–X* properties of individual fluid inclusions in the C–O–H–S system using the equations of Bakker (2003), Dubessy (1984) and Dubessy et al. (1989).

Synchrotron radiation X-ray fluorescence

Synchrotron radiation X-ray fluorescence is a non-destructive and in situ technique that allows, thanks to the high synchrotron resolution, to achieve reliable quantitative single fluid inclusion analyses. μ-SR-XRF measurements were carried out at the μ-fluorescence, μ-imaging and μ-diffraction beamline (ID22) of the European Synchrotron Radiation Facility (ESRF). A double-crystal fixed-exit monochromator was used to create a monochromatic beam of 17 keV. The beam was focused with a KB mirror to a 1.5×3 μm spot. Focused beam intensity was 3×10^{11} photons/s. X-ray fluorescence spectra were recorded with a Gresham Si(Li) detector of 140 eV resolution, placed at 90° angle to the incident beam in the polarization plane to reduce X-ray scattering. Detection of S, Cl, K and Ca was improved by placing the sample and the semiconductor detector under a helium atmosphere, which greatly reduces the absorption of low-energy fluorescence emitted by light elements.

Detailed information on the experimental protocol, absorption correction, calibration procedures and error calculations can be found in Cauzid et al. (2004, 2006), Ménez et al. (2002) and Philippot et al. (1998). As the quartz matrix absorbs elements fluorescence, elemental ratios are strongly dependent on the length of the X-ray path through the quartz (i.e. inclusion depth). To minimize this absorption, inclusions (8–20 μm in diameter) were brought to within 1–10 μm of the polished quartz surface. Calibration of the X-ray spectrum was achieved using the Cl concentration measured by microthermometry in each inclusion. When these data were not available, solutions of known composition filled in quartz capillaries were used as external standards (Cauzid et al. 2004; Mavrogenes et al. 1995). Error associated with these calibration procedures were at most ± 20%. The thickness of each inclusion and their depth relative to the polished surface were optically estimated with an error of ± 1 μm. Error on the inclusions depth propagates into a content error of 9–22% depending on the mass of the elements (Cauzid et al. 2006). Total errors were calculated using the error propagation formula detailed in Cauzid et al. (2006). These are ± 20–50% for K, Ca, Fe, Cu, Zn, Br, As, Rb and Sr (Table 2), ± 20% for Cl (from microthermometry) and 43% for Br/Cl ratios.

Oxygen isotope data

$\delta^{18}O$ data for the quartz minerals were obtained on a LaserPrep system on line to a VG Isotech (now GV instruments) Optima dual inlet (Mattey 1997) at the Royal Holloway University of London (Egham, UK). Samples (1.7 g) were combusted using a CO_2 laser in the presence of excess BrF_5. The laser spot is approximately 250 μm in diameter. The liberated O_2 passed through cryogenic traps for clean up before being directly analysed in the IRMS. Samples below 90% of the expected yield were rejected. Three mineral standards have been analysed during the runs to calibrate the data. Two are internal, GMG II (a garnet) and QBLC (a quartz) and the international NBS-30 (a biotite). All $\delta^{18}O$ values are reported relative to V-SMOW. The overall precision on standards and sample replicates is better than ± 0.1‰.

Results on fluids characteristics

Fluid inclusion textural settings and compositions

Based on textural observations and fluid compositions, three types of fluid inclusions Lw-c, Lw-1 and Lw-2 have been recognized, irrespective of the host rock lithologies. In this section we present their microthermometric, Raman spectroscopy (Table 1) and μ-SXRF analyses (Table 2).

Carbonic Lw-c fluids are common in V_1 and V_2 (Fig. 5a, b). In contrast to V_1 and V_2, V_3 contains rare and isolated Lw-c inclusions. Lw-c appear either as aligned inclusion along healed micro-fractures

Table 1 Microthermometric data and chemical compositions obtained by Raman microprobe spectrometry for Lw-c fluid inclusions

Vein type	Fluid inclusion type	Sample	H_2O (mol%)	CO_2 (mol%)	CH_4 (mol%)	Na^+ (mol%)	Cl^- (mol%)	N^2 (mol%)	D (g/cc)[a]	Dv (g/cc)[b]	Tm_{CO2}	Tm_{Clath}	Th_{CO2}
V_1	Lw-c	333-2b-f2	74	24	1	0.5	0.5		0.87	0.78	–56.9	8.9	29.2
	Lw-c	333-2b-f4	79	20		0.6	0.6		0.85	0.77	ND	8.8	28.9
	Lw-c	333-2b-f6b	71	28	0.01	0.4	0.4	0.1	0.94	0.85	–57.5		3.6
	Lw-c	333-2b-f7	30	65	0.01	1.9	1.9		0.88	0.83	–58.9	0.9	–2.4
	Lw-c	333-2b-f8	63	36		0.4	0.4		0.92	0.84	–58		2.4
V_2	Lw-c	p14-4d-f1	55	43	0.01	0.3	0.3		0.84	0.76	–57.6	9	17.1
	Lw-c	p14-4d-f4	73	25	0.01	0.6	0.6		0.89	0.76	–57.4	9	20.9
	Lw-c	p14-4d-f3b	72	27		0.4	0.4		0.92	0.81	–57.5	8.8	19.3
	Lw-c	p14-4d-f11	73	25		0.5	0.5		0.89	0.81	–56.7	9.4	30.7
	Lw-c	p14-4d-f8	13	85	0.01	0.1	0.1		0.81	0.80	–57.3		17.5
	Lw-c	p14-4f-f3	81	18		0.5	0.5		0.89	0.77	–57.7	7.8	25.8
	Lw-c	p14-4f-f1	79	20		0.5	0.5		0.92	0.81	–57.6	8.6	26.2
	Lw-c	p14-4f-f2	59	40	0.01	0.4	0.4		0.89	0.82	–57.9	8.8	10.5
	Lw-c	p14-4f-f4	13	87		0.1	0.1		0.81	0.80	–58.3	7.8	17.5
	Lw-c	p14-14e-f9	72	26	0.01	0.9	0.9		0.91	0.78	–57.7	8.2	22.8
	Lw-c	p14-14e-f5	64	35		0.6	0.6		0.78	0.77	–56.9	8.8	28.5
	Lw-c	257-2b-f10	81	16		1	1		0.95	0.79	–56.7	8.3	24.9
	Lw-c	257-2b-f11	78	19		1	1		0.93	0.78	–56.7	8.1	23.9
	Lw-c	257-2b-f12	53	47		0.2	0.2		0.91	0.85	–58.4	9.4	10.5
	Lw-c	257-2b-f13	76	23		0.4	0.4		0.91	0.78	–56.9	9.4	23.1
	Lw-c	257-2b-f14	23	76	0.01	0.1	0.1		0.85	0.83	–58.4	9.4	10.5
	Lw-c	257-2b-f18	83	11	0.01	2.5	2.5		1.01	0.77		6.5	5.6
	Lw-c	257-2b-f6	13	84	0.02	0.1	0.1	0.1	0.78	0.77	–60.8	7.3	16.9
	Lw-c	257-2b-f7	03	97					0.85	0.85	–58		9.2
	Lw-c	257-2b-f3	86	09		2.3	2.3		1.01	0.77	–57.1	6.7	22.6

[a] D = bulk density

[b] Dv = volatile phase density

terminating at the edge of a single quartz grain or as irregular clusters in quartz grains. These features support a primary or a pseudo-secondary origin. Lw-c shows CO_2 melting temperatures in the range of – 60.0 to – 56.6°C indicating the presence of anhydrous species such as CH_4, H_2S or N_2 in addition to CO_2 (Fig. 6a). Raman spectrometry revealed that CH_4 and in lesser extent N_2 are the two anhydrous species contributing to lowering the CO_2 melting temperature. Clathrate melting temperatures between 6 and 10°C (Fig. 6b) yielded salinities between 0 and 7 wt% NaCl equivalent (Fig. 8) (Collins 1979). Final homogenization in the liquid phase occurs between 234 and 272°C (Figs. 6c, 7). Decrepitation occurred between 195 and 340°C, in most cases prior to homogenization. These temperatures can be seen as minimum trapping temperatures. The wide range of decrepitation/homogenization temperature and the homogenous salinity suggest that Lw-c may have been trapped during successive stages of micro-fracturing (Fig. 7). Lw-c inclusions contain various amounts of Ca, K and transition metals (Cu, Zn, Fe) (Figs. 11, 12) and are enriched in As (up to 1,700 ppm) which is often associated with lode gold deposits. K/Rb ratio range from 2 to 400, with most data comprised between 100 and 400.

Lw-1 aqueous inclusions have been observed within a few V_1 veins and in one V_3 vein. Lw-1 occurs as inclusion trails along micro-fractures cutting across several quartz grains and primary inclusion trails (Fig. 5). Therefore Lw-1 can be seen as secondary inclusions. Ice melting temperature between – 16.1 and – 1.5°C yielded moderate salinities between 2.5 and 19.5 wt% NaCl equivalent. Homogenization temperatures of Lw-1 are within the range of 126–157°C. μ-SXRF data indicate that Lw-1 inclusions are depleted in all elements except Cl and K, and in lesser extent Ca and Fe.

Lw-2 occurs in all veins as secondary fluid inclusion trails along healed microfractures (Fig. 5). Ice melting temperature between – 6.2 and 0°C yielded salinities between 0 and 8.9 wt% NaCl equivalent with most of the analyses at around 2 wt% NaCl equivalent. Similar to Lw-1, Lw-2 homogenized in the liquid phase between 126 and 157°C. It is worth noting that in a salinity versus Td and Th diagram, Lw-1 and Lw-2 present a wide range of salinity that overlap each other (Fig. 7). This distribution may reflect an isothermal mixing process between two different fluid sources. This is further supported by the composition of Lw-2 showing a marked enrichment in K, Rb, Sr, Zn and Br when compared to Lw-1 (Fig. 11, Table 2).

Table 2 μ-SR-XRF results (ppm)

	Fluid inclusion	Cl	K	Ca	Fe	Cu	Zn	As	Br	Rb	Sr
Error (1σ)		20%	42%	40%	38%	38%	38%	38%	38%	38%	38%
Lw-1	02-211-1	26,001	6,350	1,844	115	19	23		48	20	24
	02-211-2	25,753	8,524	5,922					1,036	90	280
	02-211-3	35,721	26,865	2,581	66		8			6	4
	02-211-4	35,300	4,107	10,546	265				148	7	22
	02-211-5	53,985	8,030	5,454	111	3			123	16	43
	02-211-6	55,271	4,685	7,382	32	13			120	11	57
	02-211-7	53,344	1,677	6,085	21				101	6	45
	02-211-8	37,607	3,040	2,267	31					2	6
	02-211-9	34,663	16,525	7,208	799	8		3	144	42	78
	02-211-10	31,525	6,673	9,994	252	40	75		323	21	166
	257-1	41,730	4,111	63				5	54	18	10
	257-2	57,230	1,565	7,082	273		4	14	455	11	853
	257-3	68,692	1,857	5,424	10		7		498		
	257-4	34,615	505	1,643	3	2			99		181
	257-5	28,846	1,959	1,547	34		20	184	197	12	306
Lw-2	226-1	13,834	7,790	2,665	252		1,114	136	1,181	118	529
	226-2	22,107	9,397	4,237	685	6	2,694	176	2,088	251	863
	226-3	23,106	2,919	479	73	1	84	36	231	24	87
	226-4	27,305	3,748	1,138	205	138	478	251	146	5	79
	226-5	20,005	4,040	261	52	198	159		102	5	133
	266-6	17,364	3,603	419	97	71	75	29	125	10	142
	226-7	22,112	7,907	8,740	1,224	45	2,543	15	1,384		1,878
	226-8	23,653	30,769	1,554	998	502	2,097	4	2,252	242	895
	226-9	19,905	10,930	3,906	1,973	786	1,426		901		1,091
	226-10	33,445	4,256	1,714	99	251	306		764	31	894
	P14-1	27,269	1,471	84				3	44	4	15
	333-1	21,153	9,519		190				1,543		1,800
	03-211-1	801	317	78	27	53	39	6			
	03-211-2	4,047	740	354	47		44	33	211	38	243
	03-211-3	9,231	463	73	4	63	72	12	254	16	390
	03-211-4	3,858	1,150	188	21	88	85	41.4	277	35	423
Lw-c	P14-2	9,570	669	395	15	10		7	4		
	P14-3	9,500	1,092	175	3	6	1	4	< 1		
	P14-4	8,875	2,933	3,503	24	7	9	2			4
	P14-5	9,586	1,274		2			105	43	8	7
	P14-6	9,535	1,438	142	16		4	61	28	4	5
	P14-7	9,600	1,622					68	77	12	7
	P14-8	19,559	1,900		14		1	32	60	9	
	P14-9	1,153	133	128			1	38	47	12	4
	P14-10	9,598	861	286		7	4	128	66	8	9
	P14-11	3,384	332					29	21		
	P14-12	24,615	1,426	73	2			45	69	7	8
	P14-13	22,307	2,356	448		5		200	248	30	33
	P14-14	5,920	616	340	2				56		63
	P14-15	1,087	31	10.7	1.5			3			
	P14-16	18,956	1,155		1.6				38	3	8
	P14-17	9,417	1,200		298			35	32	3	7
	P14-18	3,341	7,827	3,217	5,357	79	324		13		36
	257-6	17,307	3,462			16		790	100	29	10
	257-7	11,252	4,111	512		681	647	16	106	37	26
	257-8	11,405	1,595	144		612	515	32	13		11
	257-9	11,198	3,185	85		1,219	946	62	20	11	18
	257-10	10,683	3,725	2,296		2,646	2,427	119	26		38
	257-11	6,067	1,230			189		179	16	10	
	257-12	11,538	1,625	172	336	128		173	94	661	149
	257-13	6,064	959	45	4	10	16	66	18		7
	257-14	11,252	4,137	1,631	91		267	140	118		114
	257-15	9,398	3,941	1,017	172	648	853	1,708			196
	257-16	10,263	3,729	196	441		183	91	94	28	46

Table 2 continued

Fluid inclusion	Cl	K	Ca	Fe	Cu	Zn	As	Br	Rb	Sr
257-17	10,256	1,774	42			1	23	16	8	
226-11	932	1,510	99	79	163	137	44	7	4	5
333-2	8,846			75	443	549		108		225
333-3	7,692			47			80	67	13	36
333-4	9,230	56	168	9		77		11		22
333-5	10,384	140	165	8		3	14	17		9
333-6	9,615	53.2	84	23	9		7	9		4
333-7	11,538	212.8	1,061	84		26	30	42	2	66
333-8	6,538	9.3	23	6	6.6					
333-9	7,692		393	42	8.8	41	13	9		9
333-10	9,336	2,296.4		374	341	249	69	12	7	27
333-11	6,529	562.8	79.4	135	111	181	23	5		10

In summary, three main fluid inclusion populations have been found within the various quartz vein families (Fig. 8). (a) Lw-c is a $H_2O - CO_2 \pm CH_4 \pm N_2$ primary fluid with a relatively high-density volatile phase, a moderate to low salinity and a significant enrichment in K and base metals. (b) Lw-1 is a moderate to high salinity aqueous fluid depleted in most trace elements. (c) Lw-2 is a low-salinity aqueous fluid showing variable enrichment in trace and major elements. On the basis of microthermometric and Raman spectroscopy, past studies of quartz carbonate veins from the Klondyke mine documented similar primary carbonic and secondary aqueous fluid inclusion populations (Huston et al. 2001).

Vein quartz oxygen isotopic composition

Oxygen isotopic compositions of vein quartz from the Warrawoona Syncline are given in Table 3. Figure 9 shows that the different types of veins display a narrow range of $\delta^{18}O$ values between + 11.5 and + 16.6‰ with a mean value at + 13.2 ± 2‰ (Fig. 9a). This suggests that quartz precipitated from a homogeneous fluid under near-isothermal conditions. The latter interpretation is reinforced by the clustered homogenization temperature distribution recorded by the primary fluid inclusions. The slightly higher $\delta^{18}O$ value of the quartz veins hosted in felsic, compared to that hosted in mafic rocks, may indicate a slight buffering by the host rock (Fig. 9b).

Discussion

Potential fluid sources

There is an ongoing debate on the source of metals and ore fluids in Archaean lode gold deposits. Three alternative sources have been suggested: (1) a meteoritic and/or seawater source (e.g. Gebre-Mariam et al. 1993; Hagemann and Ridley 1993; Nesbitt and Muehlenbachs 1989); (2) a magmatic source (e.g. Burrows et al. 1986; McNaughton et al. 1990; Meinert 1993) and (3) a metamorphic source (e.g. Fryer et al. 1979; Groves and Phillips 1987; Phillips et al. 1996). Traditionally deep sourced fluid model have been mostly favoured. However, it remains often difficult to discriminate between fluids of magmatic or metamorphic origin.

Commonly, the minimum temperature of entrapment measured for fluid inclusion is used in conjunction with the mineral oxygen isotopic composition to constrain the $\delta^{18}O$ value of the fluid from which it precipitated. In the Warrawoona Syncline, quartz veins precipitated from a near-isothermal fluid between 250 and 400°C as shown by primary fluid inclusion analyses from Lw-c. Using Zheng (1993) fractionation equation, the $\delta^{18}O$ of the fluid ranges from + 2.4 to + 12.1‰ (Fig. 10). This $\delta^{18}O$ range corresponds to a fluid in equilibrium with a crystalline basement at temperature in excess of 400–500°C. Alternatively, the vein quartz could have obtained its $\delta^{18}O$ value from the infiltration of secondary aqueous fluids. Using a fluid temperature between 120 and 160°C as shown by Lw-1 and Lw-2 measurements, the fluid $\delta^{18}O$ calculated ranges from – 7.3 to 2‰ (Fig. 10). Values around 0‰ are indicative of a meteoric or seawater-derived fluid. On a $\delta^{18}O$ versus δD diagram, the range of the quartz forming fluid $\delta^{18}O$ thus overlaps with the surfacic, magmatic and metamorphic fluid fields. It is thus essential to explore the chemistry of fluid inclusions using μ-SR-XRF.

Fluid compositions and sources

The major premise arising from individual fluid inclusion analysis using μ-SR-XRF technique is to provide

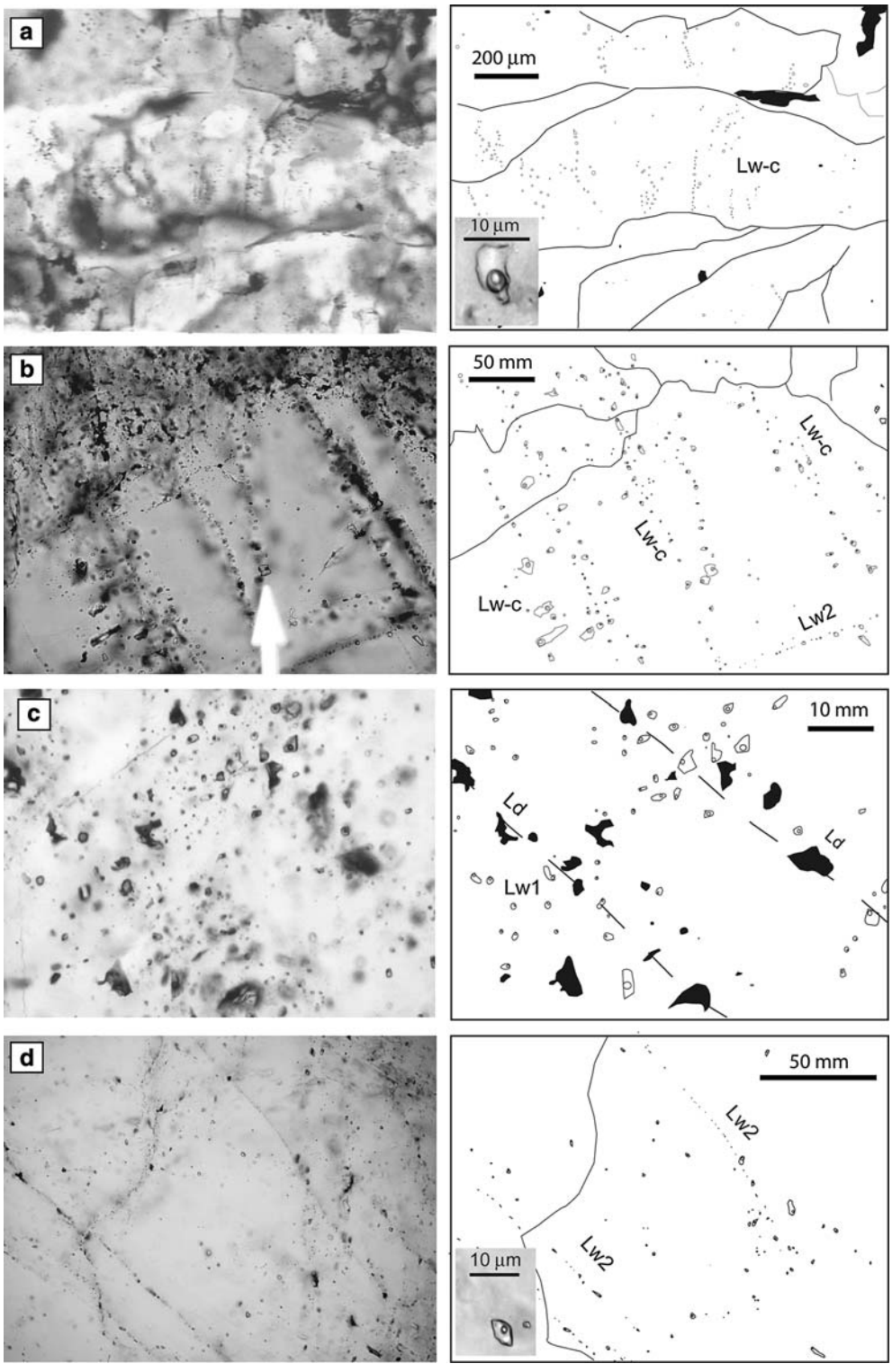

Fig. 5 Transmitted light photomicrographs and sketches of fluid inclusions from quartz veins sampled in the Warrawoona Syncline. **a** Pseudo-secondary carbonic fluid inclusions (Lw-c) trails in V_1. **b** Early secondary carbonic fluid inclusion trails (Lw-c) and aqueous secondary Lw-2 fluid inclusions in V_2. **c** Decrepitated primary fluid inclusions (Ld) located along lining overgrowth zones, and Lw-1 located along healed microfractures. **d** Secondary aqueous Lw-2 fluid inclusion trails in V_3

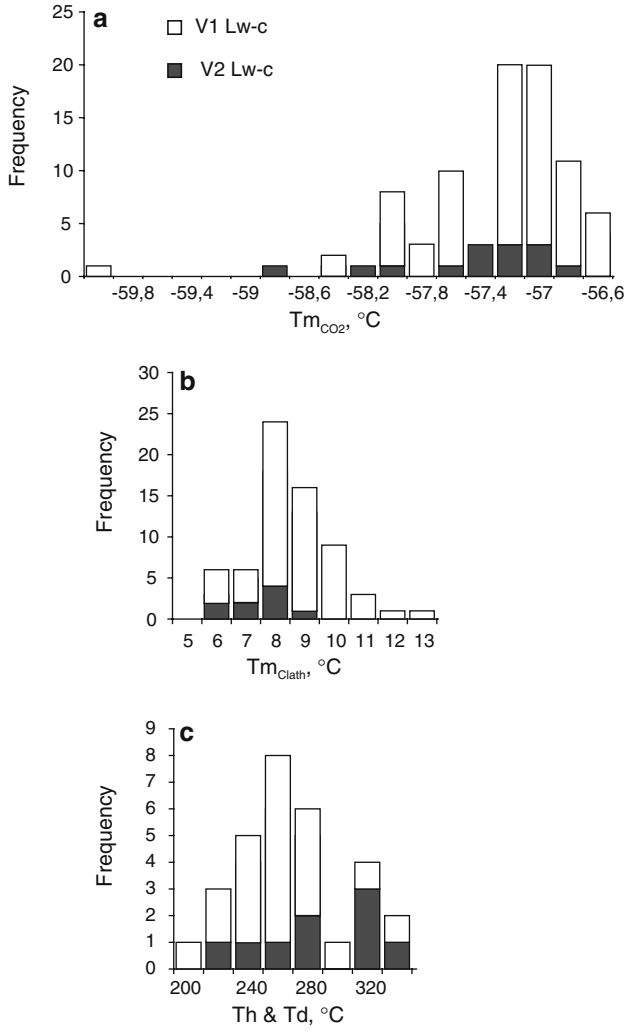

Fig. 6 Microthermometric data of Lw-c fluid inclusions from V_1 and V_2. **a** Frequency histogram of $TmCO_2$. **b** Frequency histogram of Tm_{Clath}. **c** Frequency histogram of $ThCO_2$

chemical information on the different aqueous fluids or the aqueous portion of carbonic fluid inclusions. With such information, it is then possible to discuss the composition of potential fluids reservoirs. Furthermore, some fluid reservoirs have characteristic elemental fingerprints. In addition, as the concentration of Cl and Br is higher in seawater and sedimentary aqueous brines than crustal rocks, the Cl/Br ratio is little affected by fluid–rock interaction processes and therefore can be used as a source tracer (Banks et al. 2000; Yardley and Graham 2002).

Primary fluid inclusions: Lw-c

Lw-c inclusions show a marked enrichment in K relative to Ca and Fe (Fig. 11). Potassium-rich fluids are typical magmatic sources (e.g. Bingham, UT, Butte, Montana and St. Austell, Cornwall; Irwin and Roedder 1995; Sherlock et al. 1999; Solomon et al. 2004; Zaw et al. 2003). In addition, the Cl/Br ratios measured for Lw-c fluid inclusion plots within the field of Au-bearing quartz veins from Alleghany (Böhlke and Irwin 1992) and that of volcanic fumarole condensates compiled by Böhlke and Irwin (1992) (Fig. 13). This suggests that Lw-c may be of magmatic origin. However, an additional metamorphic component is likely involved as some data plot within the field of Ouro Fino retrograde metamorphic quartz veins (Boiron et al. 1999). In addition, calculated K/Rb ratio range between 100 and 400, which overlap with the uniform crustal-like K/Rb ratio (220–400) measured in many other lode gold deposits. This uniform K/Rb ratio has been interpreted as the product of dehydration reactions within a complex lithological rock succession (Kerrich and Fryer 1988; McCuaig and Kerrich 1998), hence strongly suggesting that the Lw-c inclusions comprise an important component of metamorphic origin.

Secondary fluid inclusions: Lw-1 and Lw-2

Lw-1 inclusions are poor in Fe, base metals, metalloids or other trace elements (Fig. 12). Such a depleted fluid signature advocates for a surface origin (meteoric/seawater). On a Cl/Br versus Cl diagram Lw-1 shows a wide range of Cl/Br and Cl concentration values lining along a modern day seawater evaporation trend. In addition, Lw-1 overlaps the Canadian Shield brines field (Frape and Fritz 1987) and that of Archaean saline seawater (Foriel et al. 2004; Fig. 13). This suggests that Lw-1 represents a surface fluid with Archaean seawater affinities. In addition, in a K, Ca, Fe diagram, Lw-1 displays a wide range of composition along the K–Ca line suggesting a significant K enrichment (Fig. 11). The K enrichment as well as the lowering of the Cl/Br ratio could result from fluid interaction with felsic and/or granitic rocks involving the preferential Cl substitution in hydrous silicates. Alternatively it may highlight a fluid mixing episode with a K and Br enriched fluid.

Lw-2 inclusions are depleted in Ca but show significant enrichment in K, Zn, Sr, Rb, Br ± Cu and As (Figs. 11, 12). Lw-2 compositions are typical of granite-buffered fluids (Frape and Fritz 1987). Lw-2 shows also a significantly lower Cl/Br ratio and a marked enrichment in Br compared to Lw-c and Lw-1 (Figs. 12, 13). This high Br and low Cl content may not result from the Cl/Br fractionation due to chloride precipitation, as it does not fit the evaporation line. Alternatively, it may result from the preferential Cl substitution in

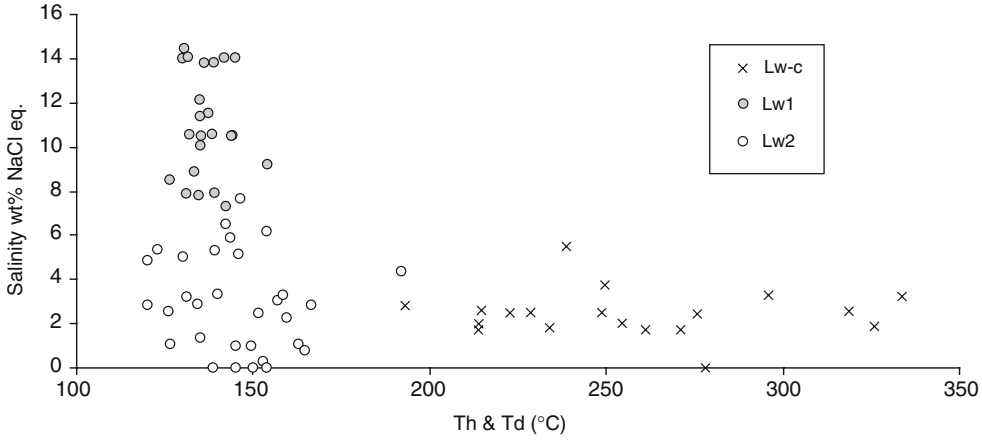

Fig. 7 Salinity versus Th and Td plot of aqueous and carbonic fluid inclusions

hydrous silicates as proposed for low-temperature brines percolating through crystalline rocks (Frape and Fritz 1987).

With regard to these results, we suggest that Lw-1 and Lw-2 fluids represent two end-members of surficial fluids, possibly of seawater origin, showing different degrees of interaction with the host rocks. According to such interpretation Lw-1 could represent a rather unbuffered pole. On the other end, Lw-2 could represent a second end-member significantly buffered by felsic and/or granitoid lithologies as attested by the low Cl/Br ratio, low salinity and high K, Sr, Rb concentrations. Accordingly, the data dispersion observed in the Cl/Br versus Cl and K, Ca, Fe diagram can either illustrate intermediate stages of fluid–rock interaction or the mixing of both fluid end-members.

Quartz vein type \ Fluid inclusion type	Lw-c	Lw-1	Lw2
	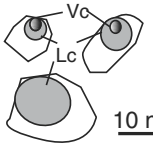	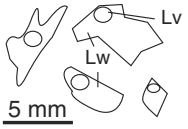	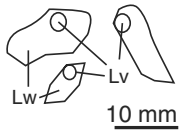
V1 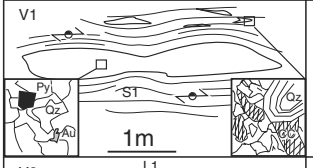	Tm_{CO_2} = -58.7 to -56.9°C Th_{CO_2} = 9.4 to 29.2 °C Tm_{Clath} = 6.1 to 9.1 °C Th = 193 to 276 °C Td = 222 to 340°C Salinity = 1 to 6.7 wt% NaCl	Tm_f = -16.1 to -2.4 °C Th = 126 to 145°C Salinity = 4.7 to 19.5 wt% NaCl eq.	Tm_f = - 4.4 to -1.8 °C Th = 123 to 146 °C Salinity = 2.5 to 7 wt%
V2 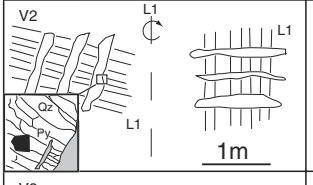	Tm_{CO_2} = -60 to -56.6 °C Th_{CO_2} = 10.5 to 32.7 °C Tm_{Clath} = 6 to 12.2 °C Th = 234 to 272 °C Td = 214 to 344 °C Salinity = 0 to 6.8 wt% NaCl	Tmf = - 14 to -1.5°C Th = 146 to 157 °C Salinity = 2.5 to 17.9 wt% NaCl eq.	Tmf = - 6.2 to 0°C Th = 120 to 163 °C Salinity = 0 to 8.9 wt% NaCl eq.
V3 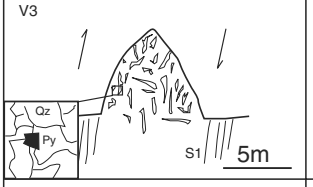	Rare isolated one Tm_{CO_2} = -56.8 °C Th_{CO_2} = 24 °C Tm_{Clath} = 8.5 °C Salinity = 6.1 wt% NaCl eq.	not present	Tmf = - 2 to 0 °C Th = 133 to 166 °C Salinity = 0 to 3.4 wt%
V4 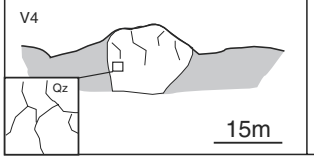	None Measured	None Measured	None Measured

Fig. 8 Synthetic diagram showing the relationship between vein type, fluid inclusion occurrence and microthermometric results

Table 3 Vein quartz oxygen isotopic values

Rock type	V_1		V_2		V_3		V_4	
	Sample	$\delta^{18}O$ (‰) ± 0.1‰	Sample	$\delta^{18}O$ (‰) ± 0.1‰	Sample	$\delta^{18}O$ (‰) ± 0.1‰	Sample	$\delta^{18}O$ (‰) ± 0.1‰
Warrawoona Syncline								
Basalt	Pb03-256	11.2	Pb03-201	12.2			Pb03-284	11.5
	Pb03-200	12.1	Pb03-296	11.9				
	Pb03-77	12.2						
	Pb03-75	12.9						
Chlorite-schist	Pb03-69	12.5	Pb03-70	13.4				
	Pb03-111	12.5	Pb03-70	13.4				
	Pb03-71	13.0	Pb03-251	13.7				
	Pb03-273	11.9						
Volcano-sedimentary layer			Pb03-63	12.4				
Breccia host rock			Pb03-66	12.2	Pb03-67	13.1		
					Pb02-226	14.0		
Ultramafic	Pb03-47	13.7	Pb03-252	12.3				
Felsic volcanics	Pb03-270	13.3	Pb03-59Q	16.1	Pb03-50Q	15.1		
			Pb03-205b	14.0	Pb03-55Q	16.6		
			Pb03-217	15.1	Pb03-214	14.6		
			Pb03-212	15.1				
Silicified basalt			Pb02-P14	14.6				
			Pb03-257	12.0				
Outside Warrawoona Syncline								
Kelly greenstone belt								
Basalt	Pb03-154	14.0					Pb03-119	12.1
Coongan greenstone belt								
Basalt	PB03-118	13.7						
Silicified basalt	Pb03-255	12.2	Pb03-319	11.4				

The veining episode

Fluid infiltration associated with the veining episode is synthesized in Fig. 14. Fluid inclusions preserved within the quartz veins document at least three fluid infiltration episodes (Fig. 14c, d). The first one is represented by primary carbonic fluid inclusions preserved within all quartz veins types. Our fluid inclusion data indicate that the fluid responsible for the vein forming fluid is of mixed magmatic and metamorphic origin. These fluids have probably been produced during the granitic dome emplacement and associated greenstone devolatilization. In this context, simple calculations show that the heat of crystallization would have released far more water through metamorphic dehydration reactions than released through the crystallizing magmas (McCuaig and Kerrich 1998). Accordingly, Lw-c fluid inclusions may record a small volume of magmatic fluid with a pronounced halogen signature mixed with large volumes of metamorphic fluids with a low halogen signature.

The second and third fluid infiltrations are highlighted, respectively, by secondary Lw-1 and Lw-2 aqueous fluid inclusion that reflect a fluid infiltration from shallow seawater reservoir. Lw-2, which is preserved in all quartz veins, is fairly similar to modern shield brines. The characteristics of Lw-2 fluids are best interpreted in terms of the interaction between a surface fluid and felsic rocks (Fig. 14b). In this regard, we suggest that the interaction of a seawater fluid (Lw-1) with crystalline rocks may have led to the formation of the Lw-2 fluid type. The percolation of these surficial fluids has likely been enhanced through a late fracturing event. Flushed within the Warrawoona Syncline, these two fluids may have mixed together thus explaining the composition range.

Lode gold mineralization implications

The fluid inclusions indicate that the fluid responsible for the lode gold mineralization was a carbonic fluid of mixed metamorphic and magmatic origin. This fluid presents similar fluid characteristics to those generally described in typical Neoarchaean orogenic lode gold deposits (e.g. Groves 1993; Groves and Phillips 1987; McCuaig and Kerrich 1998). In addition, vein quartz $\delta^{18}O$ values of + 14 ± 1‰ are also typical of many Meso- to Neoarchaean lode gold deposits (de Ronde et al. 1992; Kenich 1987; McCuaig and Kerrich 1998). Taken out of context, this fluid supports the epigenetic

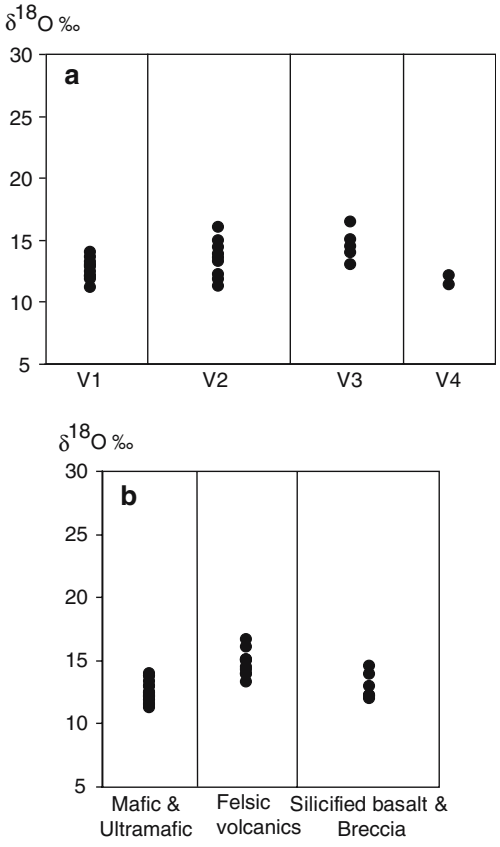

Fig. 9 Quartz $\delta^{18}O$ values of **a** the different vein types and **b** veins by different lithology sampled in the Warrawoona Syncline

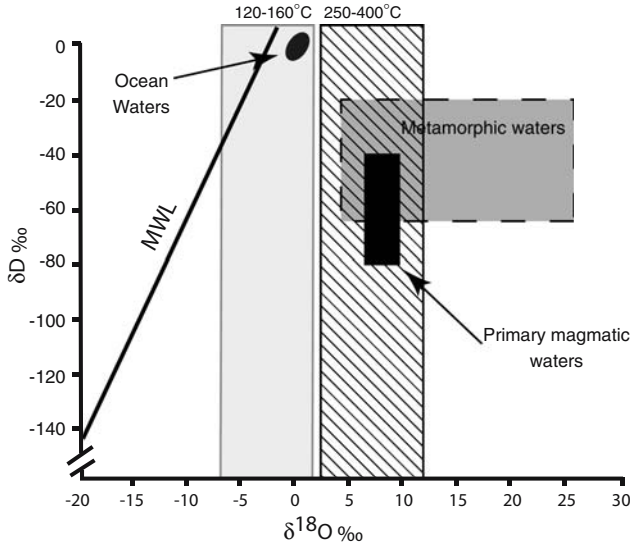

Fig. 10 δD and $\delta^{18}O$ diagram showing the fluid composition calculated from Zheng (1993) quartz fractionation equation (see text)

crustal continuum model. However, we have seen that this fluid infiltration is the last component of a polyphased and protracted fluid circulation history (Thébaud et al. 2006). This polyphased fluid circulation is not compatible with such a model.

Polyphased and protracted fluid circulation history have been documented elsewhere in the Pilbara (Zegers et al. 2002), the Barbertone Greenstone Belt

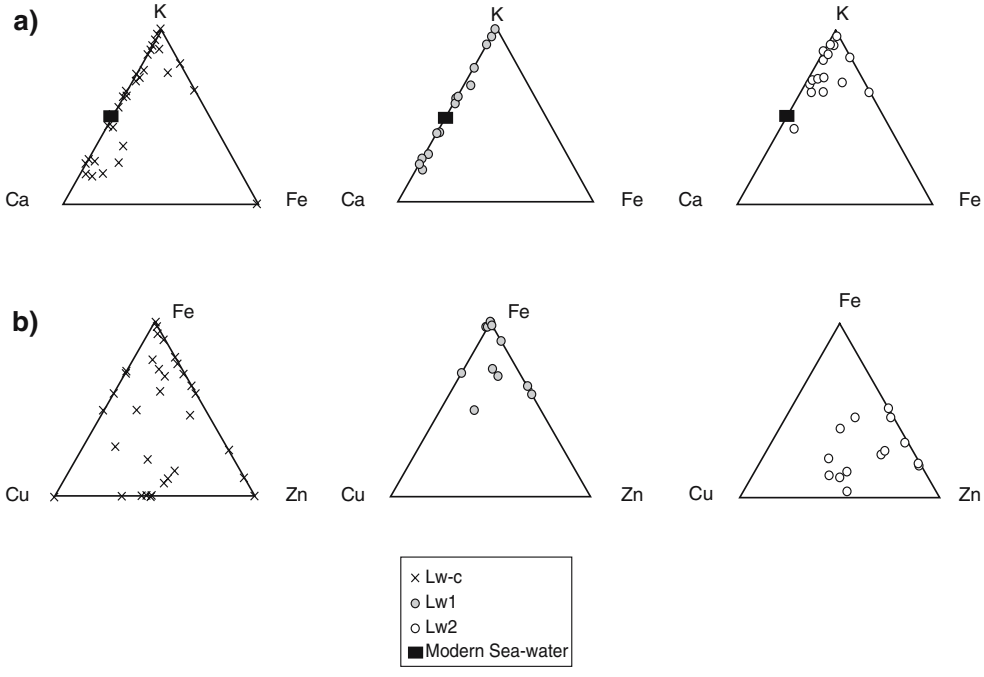

Fig. 11 μ-SR-XRF results. Individual fluid inclusion analysis shown as **a** K–Ca–Fe and **b** Fe–Cu–Zn diagrams

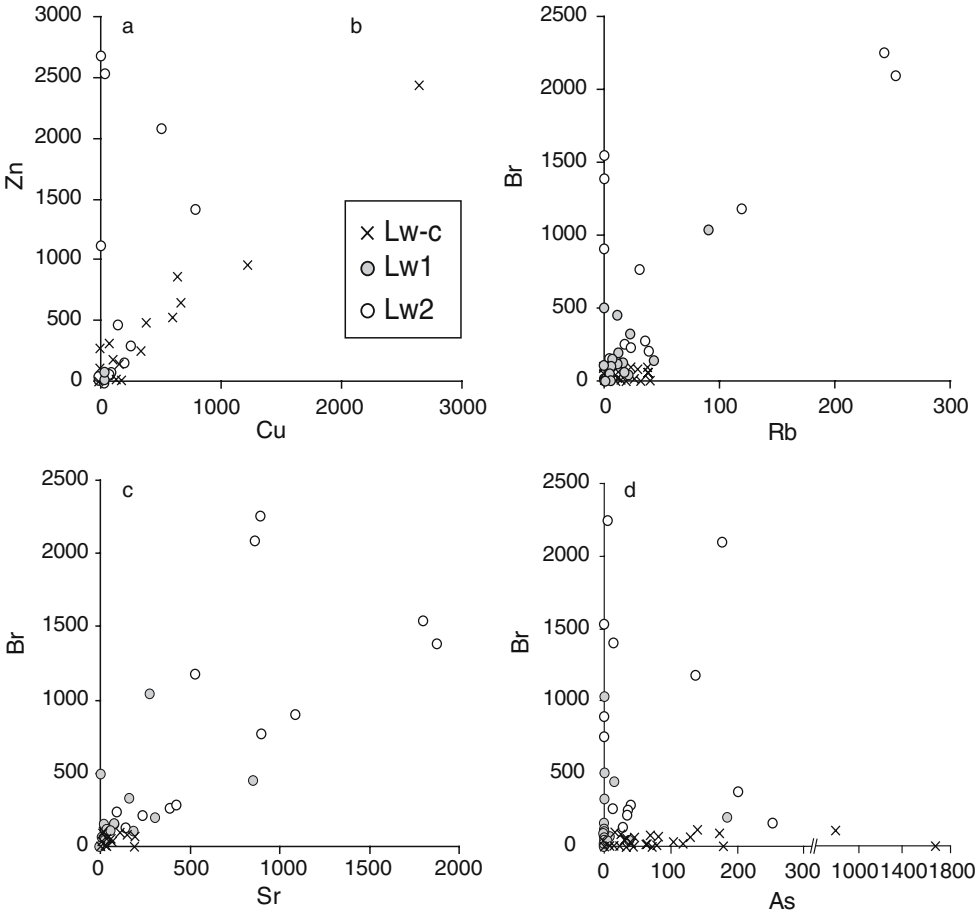

Fig. 12 μ-SR-XRF results. Individual fluid inclusion analysis. Element content in (ppm)

(Hutchinson 1993; Viljoen 1984) and the Yilgarn (Bateman and Hagemann 2004; Brown and Johnson 2003; Hutchinson 1993; Thébaud et al. 2006). It has been argued that such a polyphased and protracted genetic process is a necessary condition for the formation of economic deposits (Bateman and Hagemann 2004; Hutchinson 1993; Thébaud et al. 2006; Viljoen 1984). We suggest that the epigenetic interpretation favoured in most Archaean cratons only account for the latest fluid infiltration stage preserved in the quartz lodes, therefore missing the possible role of earlier fluid–rock interactions. In other terms, the fluid properties that characterize Archaean lode gold deposits are not discriminatory as they are compatible with both epigenetic and polyphased genetic scenarios.

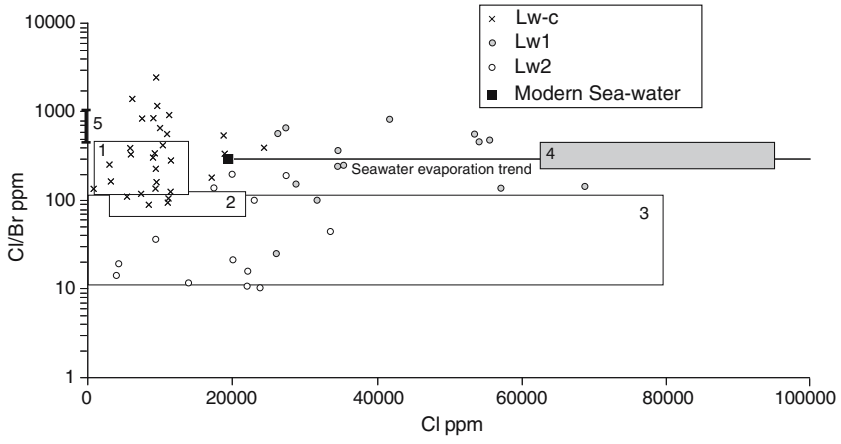

Fig. 13 μ-SR-XRF results. Individual fluid inclusion analysis. Cl/Br versus Cl with (*1*) Alleghany magmatic Au-quartz veins (Böhlke and Irwin 1992), (*2*) Ouro Fino retrograde metamorphic quartz veins (Boiron et al. 1999); (*3*) Canadian shield brines (Frape and Fritz 1987), (*4*) North Pole seawater (Foriel et al. 2004), (*5*) Volcanic fumarole condensates ranges compiled by Böhlke and Irwin (1992)

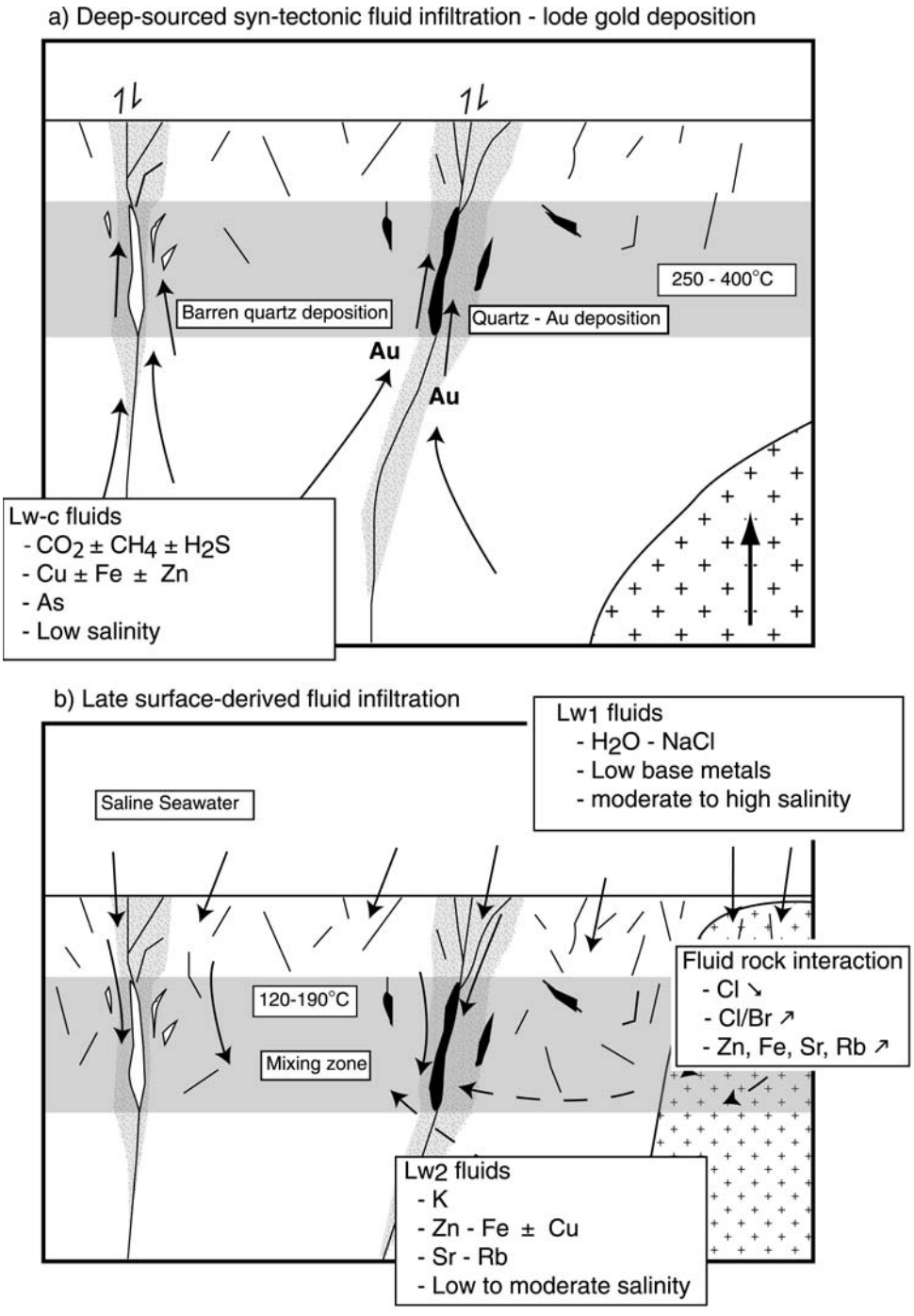

Fig. 14 Two-stage model of carbonic versus aqueous infiltration in and around the Warrawoona Syncline shear zones (**a** and **b** from Thébaud et al. 2006, see text)

Conclusion

This paper documents the fluid infiltration recorded within the syn-tectonic quartz veins associated with lode gold mineralization in the Warrawoona Syncline. Oxygen isotopic and fluid inclusion analyses including microthermometry, Raman spectroscopy and Synchrotron radiation X-ray fluorescence were used to decipher fluids composition and source. Our results suggest that three main stages of fluid infiltration were recorded in the quartz veins: a primary ore-related carbonic fluid infiltration is interpreted as of dominantly magmatic origin and two secondary aqueous fluid infiltrations of surface origin (seawater) exhibiting various levels of fluid–rock interaction. The composition of the primary fluid presents similar chemical and oxygen isotopic properties than that preserved in other Archaean lode gold deposits. However, in regard to the protracted history documented in Meso- to Neoarchean cratons, we question the robustness of

the epigenetic crustal continuum model. We suggest ore-fluid characteristics equally support an epigenetic or a polyphased mineralization process

References

Banks DA, Green R, Cliff RA, Yardley BWD (2000) Chlorine isotopes in fluid inclusions: determination of the origins of salinity in magmatic fluids. Geochim Cosmochim Acta 64:1785–1789

Bakker RJ (2003) Package FLUIDS 1. New computer programs for the analysis of fluid inclusion data and for modelling bulk fluid properties. Chem Geol 194:3–23

Bateman R, Hagemann S (2004) Gold mineralisation throughout about 45 Ma of Achaean orogenesis: protracted flux of gold in the Golden Mile, Yilgarn craton, Western Australia. Miner Depos 39:536–559

Bodnar RJ (1993) Revised equation and table for determining the freezing point depression of H_2O–NaCl solutions. Geochim Cosmochim Acta 57:683–684

Böhlke JK, Irwin JJ (1992) Laser microprobe analysis of Cl, Br, I and K in fluid inclusions: implications for sources of salinity in some ancient hydrothermal fluids. Geochim Cosmochim Acta 56:203–226

Boiron MC, Essarraj S, Sellier E, Cathelineau M, Lespinasse M, Poty B (1992) Identification of fluid inclusions in relation to their host microstructural domains in quartz by cathodoluminescence. Geochim Cosmochim Acta 56:175–185

Boiron MC, Moissette A, Cathelineau M, Banks D, Monnin C, Dubessy J (1999) Detailed determination of paleofluid chemistry: an integrated study of sulphate-volatile rich brines and aqueo-carbonic fluids in quartz veins from Ouro Fino (Brazil). Chem Geol 154:179–192

Brown SM, Johnson CA (2003) Constraints on the composition of ore fluids and implications for mineralising events at the Cleo gold deposit, Eastern Goldfields Province, Western Australia. Aust J Earth Sci 50:19–38

Burrows DR, Wood PC, Spooner ETC (1986) Carbon isotope evidence for a magmatic origin for Archaean gold–quartz vein ore deposits. Nature 321:851–854

Cauzid J, Philippot P, Somogyi A, Simionovici A, Bleuet P (2004) Quantification of single fluid inclusions by combining synchrotron radiation induced mu-X-ray fluorescence and transmission. Anal Chem 76:3988–3994

Cauzid J, Philippot P, Somogyi A, Ménez B, Simionovici A, Bleuet P (2006) Standardless quantification of single fluid inclusion analysis using synchrotron radiation induced μ-X-ray fluorescence. Chem Geol (in press)

Collins PLF (1979) Gas hydrates in CO_2-bearing fluid inclusions and the use of freezing data for estimation of salinity. Econ Geol 74:1435–1444

Collins WJ (1989) Polydiapirism of the Archean Mount Edgar Batholith, Pilbara Block, Western Australia. Precambrian Res 43:41–62

Collins WJ, Van Kranendonk MJ, Teyssier C (1998) Partial convective overturn of Archaean crust in the east Pilbara Craton, Western Australia: driving mechanisms and tectonic implications. J Struct Geol 20:1405–1424

Dubessy J (1984) Simulation des équilibres chimiques dans le système C–O–H: conséquences méthodologiques pour les inclusions fluides. Bulletins de Minéralogie 107:155–168

Dubessy J, Poty B, Ramboz C (1989) Advances in C–O–H–N–S fluid geochemistry based on micro-Raman spectrometric analysis of fluid inclusions. Eur J Mineral 1:517–534

Foriel J, Philippot P, Rey P, Somogyi A, Banks D, Ménez B (2004) Biological control of Cl/Br and low sulfate concentration in a 3.5-Gyr-old seawater from North Pole, Western Australia. Earth Planet Sci Lett 228(3–4):451–463

Frape SK, Fritz P (1987) Geochemical trends for groundwaters from Canadian shield. In: Saline water and gases in crystalline rocks, vol 33, pp 19–38

Fryer BJ, Kenich R, Hutchinson RW, Peirce MG, Rogers DS (1979) Archean precious metal hydrothermal systems, Dome mine, Abitibi greenstone belt: I. Patterns of alteration and metal distribution. Can J Earth Sci 16:421–439

Gebre-Mariam M, Groves DI, McNaughton NJ, Miicki EJ (1993) Multiple fluid sources and depositional mechanisms at the Archean mesozonal–epizonal Golden-Kilometre gold mine, Western Australia. In: Hach-Ali F, Tortes-Ruiz J, Gervilla F (eds) Current research in geology applied to gre deposits, pp 453–456

Goldfarb RJ, Groves DI, Gardoll S (2001) Orogenic gold and geologic time: a global synthesis. Ore Geol Rev 18:1–75

Groves D (1993) The crustal continuum model for late Archaean lode-gold deposits of the Yilgarn Block, Western Australia. Miner Depos 28:366–374

Groves DI, Phillips GN (1987) The genesis and tectonic control on Archaean gold deposits of the western Australian shield—a metamorphic replacement model. Ore Geol Rev 2:287–322

Hagemann SG, Ridley JR (1993) Hydrothermal fluids in epiand kataxonal crustal levels in the Archaean: implications for P-T-X-f evolution of lode-gold mineralisation. In: Williams PR, Haldane JA (eds) Kalgoorlie'93: an international conference on crustal evolution, metallogeny and exploration of the Eastern Goldfields, vol 54. Amt. Geol. SW. Organ. Record 1993, pp 123–130

Hickman AH (1983) Geology of the Pilbara Block and its environs. 1981/36, vol 127. Geological Survey of Western Australia, Perth, p 268

Hickman AH (2001) East Pilbara diapirism: new evidence from mapping. West Aust Geol Surv Rec 5:23–25

Hickman AH, Van Kranendonk MJ (2004) Diapiric processes in the formation of Archaean continental crust, East Pilbara Granite–Greenstone Terrane, Australia. In: Eriksson PG, Altermann W, Nelson DR, Mueller WU, Catuneanu O (eds) Tempos and events in Precambrian time. Elsevier, Amsterdam, pp 54–75

Huston D, Blewett R, Mernaugh T, Sun S-S, Kamprad J (2001) Gold deposits of the Pilbara Craton: results of AGSO Research, 1998–2000, vol 10, p 32

Hutchinson RW (1993) A multi-stage, multi-process genetic hypothesis for greenstone-hosted gold lodes. Ore Geol Rev 8:349–382

Irwin JJ, Roedder E (1995) Diverse origins of fluid in magmatic inclusions at Bingham (Utah, USA), Butte (Montana, USA), St Austell (Cornwall, UK), and Ascension Island (mid-Atlantic, UK), indicated by laser microprobe analysis of Cl, K, Br, I, Ba + Te, U, Ar, Kr, and Xe. Geochim Cosmochim Acta 59:295–312

Kenich R (1987) The stable isotope geochemistry of Au–Ag vein deposits in metamorphic rocks. In: Kyser TK (ed) Mineralogical Association of Canada Short Course, vol 13, pp 287–336

Kerrich R, Fryer BJ (1988) Lithophile-element systematics of Archaean greenstone belt Au–Ag vein deposits: implications for source processes. Can J Earth Sci 25:945–953

Kerrich R, Wyman D (1990) Geodynamic setting of mesothermal gold deposits: an association with accretionary tectonic regimes. Geology 18:882–885

Kloppenburg A, White SH, Zegers TE (2001) Structural evolution of the Warrawoona Greenstone Belt and adjoining granitoid complexes, Pilbara Craton, Australia: implications for Archaean tectonic processes. Precambrian Res 112:107–147

Mattey DP (1997) LaserPrep: an automatic laser-fluorination system for micromass 'Optima' or 'Prism' mass spectrometers, p 8

Mavrogenes JA, Bodnar RJ, Anderson AJ, Bajt S, Sutton SR, Rivers ML (1995) Assessment of uncertainties and limitations of quantitative elemental analysis of individual fluid inclusions using synchrotron X-ray fluorescence (SXRF). Geochim Cosmochim Acta 59:3987–3995

McCuaig TC, Kerrich R (1998) P-T-t-deformation-fluid characteristics of lode gold deposits: evidence from alteration systematics. Ore Geol Rev 12:381–453

McNaughton NJ, Barley ME, Cassidy KF, Golding SD, Groves DI, Ho SE, Hronsky JM, Sang JH, Turner JV (1990) Gold deposits of the Archaean Yilgam Block, Western Australia: nature, genesis and exploration guides. In: Ho SE, Groves, D.I., Bennett JM (eds) Carbon isotope studies, vol 20. Geol. Dep. Univ. Extension, Univ. Western Australia Publ., pp 246–251

Meinert LD (1993) Igneous petrogenesis and skarn deposits. In: Kirkham RV, Sinclair WD, Thorpe RI, Duke JM (eds) Mineral deposit modeling, vol 40. Geol. Assoc. Can., Spec. Pap., pp 569–583

Ménez B, Philippot P, Bonnin-Mosbah M, Simionovici A, Gibert F (2002) Analysis of individual fluid inclusions using synchrotron X-ray fluorescence microprobe: progress toward calibration for trace elements. Geochim Cosmochim Acta 66:561–576

Nesbitt BE, Muehlenbachs K (1989) Origins and movement of fluids during deformation and metamorphism in the Canadian Cordillera. Science 245:733–736

Philippot P, Ménez B, Chevalier P, Gibert F, Legrand F, Populus P (1998) Absorption correction procedures for quantitative analysis of fluid inclusions using synchrotron radiation X-ray fluorescence. Chem Geol 144:121–136

Phillips GN, Groves DI, Kerrich R (1996) Factors in the formation of the giant Kalgoorlie gold deposit. Ore Geol Rev 10:295–317

Roedder E (1972) Composition of fluid inclusions. In: Fleischer M (ed) Data of geochemistry, 6th edn. US Geological Survey professional paper 440JJ

de Ronde CEJ, Spooner ETC, de Wit MJ, Bray CJ (1992) Shear zone-related, Au quartz vein deposits in the Barberton greenstone belt, South Africa: field and petrographic characteristics, fluid properties and light stable isotope geochemistry. Econ Geol 87:366–402

Sherlock RL, Roth T, Spooner ETC, Bray CJ (1999) Origin of the Eskay Creek precious metal-rich volcanogenic massive sulfide deposit: fluid inclusion and stable isotope evidence. Econ Geol 94:803–824

Smithies RH, Champion DC, Cassidy KF (2003) Formation of Earth's early Archaean continental crust. Precambrian Res 127:89–101

Solomon M, Gemmell JB, Zaw K (2004) Nature and origin of the fluids responsible for forming the Hellyer Zn–Pb–Cu, volcanic-hosted massive sulphide deposit, Tasmania, using fluid inclusions, and stable and radiogenic isotopes. Ore Geol Rev 25(1–2):89–124

Teyssier C, Collins WJ, Van Kranendonk MJ (1990) Strain and kinematics during the emplacement of the Mount Edgar Batholith and Warrawoona Syncline, Pilbara Block, Western Australia. In: Geoconferences (W.A.), Perth, Western Australia, pp 481–483

Thébaud N, Philippot P, Rey P, Brugger J, Kranendonk MV, Grassineau N (2006) Protracted fluid–rock interaction in the mid-Archaean and implication for gold mineralization: example from the Warrawoona Syncline (WA). Earth Planet Sci Lett (submitted)

Van Kranendonk MJ, Hickman AH, Smithies RH, Nelson DR, Pike G (2002) Geology and tectonic evolution of the Archaean North Pilbara Terrain, Pilbara Craton, Western Australia. Econ Geol 97(4):695–732

Van Kranendonk MJ, Smithies RH, Hickman AH, Bagas L, Williams IR, Farrell TR (2004) Event stratigraphy applied to 700 million years of Archaean crustal evolution, Pilbara Craton, Western Australia. In: Technical papers 2003-04 annual review. Geological Survey of Western Australia, Perth, pp 49–61

Viljoen M (1984) Archaean gold mineralization and Komatiites in Southern Africa. In: Foster RP (ed) Gold'82: the geology, geochemistry and genesis of gold deposits. A A Balkema, Rotterdam

Yardley BWD, Graham JT (2002) The origins of salinity in metamorphic fluids. Geofluids 2:249–256

Zaw K, Hunns SR, Largea RR, Gemmella JB, Ryanb CG, Mernagh TP (2003) Microthermometry and chemical composition of fluid inclusions from the Mt Chalmers volcanic-hosted massive sulfide deposits, central Queensland, Australia: implications for ore genesis. Chem Geol 194:225–244

Zegers TE, Barley ME, Groves DI, McNaughton NJ, White SH (2002) Oldest gold: deformation and hydrothermal alteration in the Early Archean Shear Zone-hosted Bamboo Creek Deposit, Pilbara, Western Australia. Econ Geol 97(4):757–773

Zheng YF (1993) Calculation of oxygen isotope fractionation in anhydrous silicate minerals. Geochim Cosmochim Acta 57:1079–1091